This is a repository copy of *Redox-switchable siderophore anchor enables reversible artificial metalloenzyme assembly*.

Redox-switchable Siderophore Anchor Enables Reversible Artificial Metalloenzyme Assembly

Daniel J. Raines,[1] Justin E. Clarke,[1,2] Elena V. Blagova,[2] Eleanor J. Dodson,[2] Keith S. Wilson[2]* and Anne-K. Duhme-Klair[1]*

[1]Department of Chemistry, University of York, Heslington, York, YO10 5DD, United Kingdom

[2]Structural Biology Laboratory, Department of Chemistry, University of York, Heslington, York, YO10 5DD, United Kingdom

Table of contents:
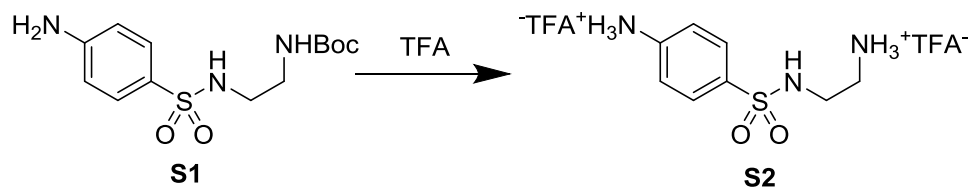
Supplementary Methods

Supplementary Tables

Supplementary Figures

Supplementary References

Supplementary Methods

a. Synthesis and characterisation of additional compounds

Synthesis of Compound **S2**.

To a stirred solution of compound **S1** (0.35 mmol, 0.1127 g, prepared in accordance to the literature[1]) dissolved in 8 mL dry MeOH, 2 mL trifluoroacetic acid was added and the mixture was stirred overnight. The volatiles were removed *in vacuo* and the residue taken up in 5 mL dry EtOH which was subsequently removed *in vacuo*. This process was repeated 5 times to yield **S2** as a brown solid (0.1213 g, 0.27 mmol, 78%), which was used for the preparation of a 10 mM stock solution of **3** for catalytic activity testing, as detailed in the methods section.

TLC (EtOAc 100%): R_f = 0; ^{1}H NMR (400 MHz, (CD$_3$)$_2$SO): δ 7.91-7.70 (m, 4H), 7.42 (d, J = 8.5 Hz, 2H), 7.35 (t, J = 5.5 Hz, 1H), 6.62 (d, J = 8.5 Hz, 2H), 6.01 (br s, 1H), 2.90-2.75 (m, 4H); HRMS (*m/z*): [M+H][+] calcd. for C$_8$H$_{14}$N$_3$O$_2$S, 216.0801; found, 216.0799.

Synthesis of (*R*)-(+)-Salsolidine. (*R*)-(+)-Salsolidine was prepared in accordance to the literature.[2] $[α]^{20}_D$ = +46.6 (*c* 1.0, EtOH), lit. $[α]^{20}_D$ = +51.0 (*c* 1.0, EtOH).[3]

b. Circular dichroism spectroscopy

Samples were prepared in a 1 cm quartz cuvette. Spectra were recorded in continuous mode with a range of 300-700 nm, 0.5 nm pitch, 100 nm/min scanning speed, 2 s response, 2 nm bandwidth, and 3 accumulations. A blank buffer sample of 100 mM Tris pH 7.5, 150 mM NaCl was recorded first. Final Fe(III)-azotochelin, Fe(III)-azotochelin-catalyst conjugate and CeuE concentrations were 70 µM. The blank spectrum was subtracted from all sample spectra.

c. Intrinsic fluorescent quenching titrations

Spectra were recorded with an excitation of 280 nm, emission range of 295-410 nm, 10 nm excitation slit width, 10 nm emission slit width, 60 nm/min scanning speed, automatic response, corrected spectra and 950 V detector voltage. For each sample, 2 mL of 240 nM CeuE in 40 mM Tris-Cl pH 7.5, 150 mM NaCl were placed in a 1 cm quartz cuvette and titrated stepwise with 120 µM ligand solution using a DOSTAL DOSY liquid dispenser with continuous stirring. After each addition, the solution was allowed to equilibrate for 1 minute before scanning. Fluorescence spectra were buffer subtracted and integrated between 305-355 nm, with the peak area plotted as a function of ligand concentration. Final K_d values were obtained using DynaFit.[4] Final K_d values for CeuE were determined as $[Fe^{III}(AZOTO)]^{2-}$ 4.9 ± 0.4 nM, $[Fe^{III}(solv)_2(\textbf{11})Cp^*Ir^{III}Cl]^-$ 18.3 ± 4.9 nM, and for CeuE H227A and $[Fe^{III}(solv)_2(\textbf{11})Cp^*Ir^{III}Cl]^-$ 22.9 ± 11.6 nM.

The binding of apo-azotochelin (the anchor unit) and Fe(II)-azotochelin to CeuE were investigated for comparison and their binding affinities were found to be significantly lower (>1 µM) than that of $[Fe^{III}(AZOTO)]^{2-}$ (Supplementary Figure 1). The initial

decrease in emission seen in the aerobic apo-azotochelin fluorescence quenching titration curve is due to a contamination of the azotochelin sample with iron(III); it is very difficult to obtain siderophores that are completely iron free. The solutions for the Fe(II)-azotochelin fluorescence quenching titration were prepared anaerobically using Schlenk techniques and with ferrous sulfate as the iron source. The titration was carried out in a closed cuvette equipped with a Suba seal and with a gas-tight syringe under an atmosphere of nitrogen.

d. Electrospray ionization mass spectrometry

ESI-MS was performed using an ABI Qstar tandem mass spectrometer. Samples were prepared by dilution in 40 mM Tris-Cl pH 7.5, 150 mM NaCl to a final concentration and volume of 400 µM and 30 µL, respectively. Samples were then dialysed in 40 mM Tris-Cl pH 7.5, 150 mM NaCl for 2 h, followed by dialysis in 2 mM Tris-Cl pH 7.5 for a further 2 h. Samples were then diluted 200-fold in 5 mM ammonium acetate pH 4.5, 3.5% (v/v) methanol and analysed via mass spectrometry. Data were processed to yield final mass values and corrected with reference to an external myoglobin standard.

The data derived from the lower 810-2000 m/z range of the raw data (usually associated with unfolded protein, Supplementary Figure 3 red) were used to determine the accurate mass of the ions present, with signals observed at 32024.4 and 33078.4 Da, consistent with CeuE and $[Fe^{III}(\mathbf{11})Cp^*Ir^{III}] \subset CeuE$ (theoretical mass 32024.0 and 33079.0, respectively; see below for calculations). These peaks were compared to the spectra derived from the higher 2000-2400 m/z range of the raw data (usually associated with native, folded protein, Supplementary Figure 3 blue).

Notably, the native traces suggest that the majority of the species in the CeuE-conjugate sample are the fully intact [Fe^{III}(**11**)Cp*Ir^{III}]⊂CeuE with little unbound CeuE. However, the accuracy of the molecular weights in these spectra is limited due to the data being processed outside the calibration range of the system.

The theoretical average mass for CeuE was calculated using the ExPASy online calculator by inputting the amino acid sequence 44-330 of *C. jejuni* CeuE (UniProt Q0P8Q4) with an additional glycine-proline-alanine-leucine sequence at the N-terminus of the protein, a remnant of the N-terminal hexa-histidine tag. The predicted molecular weight given was 32024.0 Da. The theoretical average mass for [Fe^{III}(**11**)Cp*Ir^{III}]⊂CeuE was calculated by addition of the theoretical average mass of CeuE to the theoretical average mass of the [Fe^{III}(**11**)Cp*Ir^{III}] (1056 Da) and subtracting 1 Da due to the loss of a proton from the Tyr288 upon coordination to the Fe(III). This yielded a final theoretical average mass of 33079.0 Da.

e. Crystal structure determinations

Protein crystallography. Attempts to co-crystallise the iron(III) complexes of azotochelin or the Ir conjugate with CeuE were unsuccessful, so the two compounds were independently soaked into apo crystals, which are in space group P1 with three independent protein molecules in the asymmetric unit. For the azotochelin structure, the apo-CeuE crystal was grown from 0.2 M sodium fluoride, 20% PEG 3350 before soaking with ferric-azotochelin (5 mM) overnight. Ferric-azotochelin was prepared by mixing 80 μL of azotochelin (500 mM in DMF), 80 μL of iron(III) chloride hexahydrate (500 mM in H$_2$O) and 80 μL of sodium hydroxide (1 M in H$_2$O) in 560 μL DMF. The resulting 50 mM ferric-azotochelin stock (1 μL) was then mixed with the well solution

(10 µL) and clarified by centrifugation. The clarified stock (0.8 µL) was added to the protein drop with the crystal and allowed to soak for 20 hours. The crystal was vitrified at 110 K using the well solution with increased concentration of PEG 3350 (33%) as cryoprotectant.

For the structure with the conjugate the best results were obtained after soaking for 24 hours into a crystal grown in the condition 0.1 M succinic acid, sodium dihydrogen phosphate and glycine, pH 9, 25% PEG 1500. The conjugate DMF stock was prepared by mixing a stirred solution of **11** (5 µM in MeOH, 1 mL) with iron(III) chloride hexahydrate (5 µM in MeOH, 1 mL) for 30 minutes at room temperature, followed by the addition of $[Ir(Cp^*)(Cl)_2]_2$ (2.5 µM in MeOH, 1 mL) and stirred for 18 hours. The solvent was removed *in vacuo* and the residue was dissolved in 100 µL DMF. The soaking procedure for the conjugate was the same as for ferric-azotochelin (NB. precipitate formation was more pronounced upon addition of the conjugate solution to the well solution, therefore after centrifugation only the supernatant was used for soaking). Crystals were vitrified at 110 K without additional cryoprotectant.

Data for the azotochelin and conjugate structures were recorded at beam lines I03 and I04, respectively of the Diamond Light Source. Data integration was carried out with XDS[5] through Xia2[6] and the data were merged with Aimless[7] and computations were carried out with programs from the CCP4 suite[8]. Details of the data collection and refinement are given in Supplementary Table 1. Both structure solutions started from placing the model of the 4-LICAM CeuE complex (PDB 5A1J) using MOLREP[9], and refinement and rebuilding were carried out using REFMAC5[10] and COOT[11].

The unit cell dimensions are shown in Supplementary Table 2 for these crystals and the apo form (3ZKW). The most significant variation is a change in α of about 5° for the iridium conjugate [Fe^{III}(**11**)Cp*Ir^{III}]. The crystals of the linear dimer complex (PDB 5ADV and 5ADW) have similar dimensions to the apo and [Fe^{III}(AZOTO)]$^{2-}$ complex.

In the azotochelin complex, the initial difference maps showed density for the ligand and associated iron in chains A and B (Supplementary Figure 2) with no ligand in chain C, similar to the binding of the linear dimer to CeuE (PDB 5ADV and 5ADW). The ligand was built into the density and the structure refined.

The cell dimensions of the conjugate [Fe^{III}(**11**)Cp*Ir^{III}] are somewhat different to those of *apo*-CeuE, the linear dimer and azotochelin. In this complex, the conjugate is bound to chains A and C, being more highly ordered in the latter.

The anomalous difference synthesis guided our interpretation. There are anomalous difference peaks corresponding to the expected position of the iron in Chains A and C. The peak height of these gave us a baseline for estimating the iridium occupancies. There are three equidistant pairs of peaks that can be assumed to be iridium ions, present in all three chains. The partial occupancies of the pairs of iridium atoms are estimated to be for A: 0.3, 0.3, for B: 0.1, 0.1 and for C: 0.6, 0.3 (Supplementary Figure 4). The peak height of the major C site is about three times that of the iron, consistent with an estimated iridium occupancy of 0.6, subsequently confirmed during refinement. Similar partial occupancies have previously been observed previously in crystal structures of ATHases with anchored iridium-based catalysts.[12,13]

The conjugate ligand was generated using Acedrg[14] in three segments, corresponding to the azotochelin moiety, the catalyst moiety and the cyclopentadienyl, allowing the first part to be modelled at full occupancy with the latter two as 0.6, equivalent to that refined for the major iridium site. Restraints around the iridium were based on the parameters observed in the small molecule structure of the catalyst (CCDC 1551724). The initial difference density map for the conjugate bound to chain C is shown in Supplementary Figure 5, with the final model for the ligand superposed. The azotochelin portion was assigned an occupancy of 1, the rest of the ligand 0.6.

Small molecule crystallography. Diffraction quality crystals were obtained by slow diffusion of diethyl ether into a solution of $[Cp*Ir^{III}(\mathbf{6})Cl]$ (**12**) in chloroform. Crystallographic data were collected on an Oxford Diffraction SuperNova diffractometer with Mo-K_α radiation (λ = 0.71073 Å) using an EOS CCD camera. The crystals were cooled with an Oxford Instruments Cryojet. Face-indexed absorption corrections were applied using SCALE3 ABSPACK scaling. OLEX2[15] was used for overall structure solution, refinement and preparation of computer graphics and publication data. Within OLEX2, the algorithms used for structure solution were direct methods using SHELXS-97 and refinement by full-matrix least-squares used SHELXL-97 within OLEX2. All non-hydrogen atoms were refined anisotropically. H-atoms were placed using a riding model and included in the refinement at calculated positions. Crystallographic data are summarised in Supplementary Table 3.

f. Reversibility studies

[Fe^{III}(AZOTO)]$^{2-}$⊂CeuE. Spectra were recorded between 220-1000 nm on a Shimadzu UV-1800 in a Type 18/B/9 quartz cuvette (Starna scientific). The sample was prepared by mixing 245 µL of 0.1 M MES, 0.5 M NaCl pH 6.0 with 2.5 µL azotochelin (10 mM, DMSO) and 2.5 µL Fe(NTA) (10 mM, H$_2$O, prepared in accordance to the literature[8]) (Supplementary Figure 7, A). To this solution, 14 µL CeuE (65 mgmL^{-1} in 0.1 M MES, 0.5 M NaCl pH 6.0) was added and the purple solution was gently mixed (Supplementary Figure 7, B). Then 2.5 µL Na$_2$S$_2$O$_4$ (0.5 M, H$_2$O) were added and the solution was gently mixed until the solution appeared colourless, indicating that the reduction reaction was complete (Supplementary Figure 7, C). A 40 µL aliquot of this solution was removed and added to 160 µL of ferrozine stock solution (0.2 mM, 0.1 M MES, 0.5 M NaCl pH 6.0), gently mixed with an additional 1 µL Na$_2$S$_2$O$_4$ to fully reduce any additional oxidants present in the buffer (Supplementary Figure 7, D). To re-oxidise the sample, air was slowly bubbled through the remaining 210 µL of the solution until complete oxidation was apparent due the resulting purple colour of the solution (Supplementary Figure 7, E). After re-oxidation, a 40 µL aliquot of the sample was removed and added to 160 µL of ferrozine stock solution (0.2 mM, 0.1 M MES, 0.5 M NaCl pH 6.0) and gently mixed (Supplementary Figure 7, F).

[Fe^{III}(11)Cp*Ir^{III}]⊂CeuE. *a) Protein recycling:* Samples were prepared by mixing 1780 µL of 0.1 M MES pH 6, 0.5 M NaCl with 200 µl of [Fe^{III}(**11**)Cp*Ir^{III}]⊂CeuE (40 mgmL^{-1} in 0.1 M MES pH 6, 0.5 M NaCl). To this solution, 20 µL of Na$_2$S$_2$O$_4$ (1 M, H$_2$O) was added and the solution was mixed gently until it appeared colourless. The solution was then concentrated in Vivaspin 500 centrifugal concentrators (10 kDa MWCO) via centrifugation at 10,000 x *g* for 10 min under nitrogen flux. Samples of around 25 µL

were present in the retained fractions, which were pooled and tested for protein via Bradford assay quantification. The retained CeuE was loaded with fresh [Fe^{III}(**11**)Cp*Ir^{III}] at 1:1 molar ratios in the same manner as before. Catalytic assays were performed as before, but with a final catalyst/artificial enzyme concentration of 0.05 mM. Protein integrity during several key steps of the metalloenzyme reassembly was confirmed by SDS-PAGE (Supplementary Figure 8).

Protein confirmation upon dissociation of the metalloenzyme was confirmed by circular dichroism in the UV range. Samples were prepared by dialysis in 5 mM Tris-Cl pH 7.5 at final protein concentrations of around 0.2 mg mL^{-1}. Samples were analysed in a 0.1 cm quartz cuvette. Spectra were recorded in continuous mode with a range of 190-260 nm, 0.5 nm pitch, 100 nm/min scanning speed, 2 s response, 2 nm bandwidth, and 3 accumulations. A blank buffer sample of 5 mM Tris pH 7.5 was recorded first. Final protein concentrations were determined using a Bradford assay. The blank spectrum was subtracted from all sample spectra and the raw data were then converted to molar ellipticity values using Supplementary Equation (1):

$$[\theta] = (mdeg * Mw)/(10 * C * l) \qquad\qquad (1)$$

Where $[\theta]$ is the molar ellipticity, $mdeg$ is the raw millidegree value, Mw is the average molecular weight of the protein in gmol^{-1}, C is the protein concentration in gL^{-1}, and l is the path length of the cuvette in cm.

b) Azotochelin-catalyst conjugate extraction and recycling: To a 300 μL sample of [Fe^{III}(**11**)Cp*Ir^{III}]⊂CeuE (1 mM in 0.1 M MES pH 6, 0.5 M NaCl), Na$_2$S$_2$O$_4$ (1 M, H$_2$O) was added until the solution appeared colourless, followed by immediate extraction with ethyl acetate (3 x 500 μL). During the second extraction step precipitation of CeuE was observed. The combined organic extracts were filtered through a 0.22 μm

PTFE membrane and analysed by ESI MS (m/z [M-H]$^-$ calcd. for $C_{33}H_{34}N_5O_9S$ 676.2083, found 676.2103; calcd. for $C_{27}H_{29}N_4O_9S$ 585.1661, found 585.1678, calcd. for $C_{27}H_{28}N_3O_7$ 506.1933, found 506.1946) and HPLC (Athena C-18 column, 100 Å pore size, solvent A: H_2O + 0.1% formic acid, solvent B: MeCN + 0.1% formic acid, gradient 5-95% B over 15 min, 1 mL/min flow rate, 20 µL injection volume, 30 °C). Retention times are as follows, with peaks assigned by comparison with a mixture of relevant standards: 8.08 min H_5-**11**, 8.53 min, iridium-bound azotochelin-catalyst conjugate; recovery yields of 15% and 11%, respectively (Supplementary Figure 9a).

Catalytic activity testing: the organic azotochelin-catalyst conjugate extract was evaporated to dryness and the ATHase was reconstituted by addition of Fe(III)-NTA, [Cp*Ir^{III}Cl$_2$]$_2$ and CeuE solutions to restore equimolar ratios of Fe(III), Ir(III), conjugate and CeuE in the same manner as before. Catalytic assays were performed as described for the recycled protein above using an artificial ATHase concentration of 0.05 mM (Supplementary Fig. 9b).

Supplementary Tables

Supplementary Table 1. Crystallographic statistics[a].

Crystal	[Fe^{III}(AZOTO)]$^{2-}$	[Fe^{III}(**11**)Cp*Ir^{III}]
PDB-entry	5OAH	5OD5
Beamline	Diamond I04	Diamond I03
Wavelength (Å)	0.9795	0.9762
Space group	P1	P1
Cell parameters (Å and °)	a=58.14 b=63.41 c=67.67	a=55.61 b=62.76 c=68.20

	α=82.71 β=76.36 γ=79.03	α=87.38 β=76.90 γ=79.27
Resolution range (Å)	65.5–1.80	40.97–1.80
Outer range (Å)	1.83–1.80	1.83-1.80
Number of reflections	429,701	548,869
Unique reflections	84,430	83,133
Monomers in asymmetric unit	3	3
Completeness (%)	99.1 (97.9)	99.7 (100.0)
$I/I(\sigma)$	13.3 (2.2)	7.4 (1.1)
CC(1/2)	0.998 (0.867)	0.997 (0.502)
Average multiplicity	5.1 (5.3)	6.6 (6.4)
R_{merge} (%)[b]	5.5 (74.0)	11.3 (162.2)
Percentage of R_{free} reflections (%)	5.00	5.00
$R_{cryst} = \Sigma\left||F_o|-|F_c|\right|/\Sigma|F_o|$ (%)	20.6	18.0
Free R factor (%)	25.2	20.7
Bond distances[c] (Å)	0.019 (0.019)	0.022 (0.019)
Bond angles (°)	1.949 (1.987)	2.026 (1.986)
Chiral centres (Å^3)	0.118 (0.200)	0.141 (0.200)
Planar groups (Å)	0.009 (0.021)	0.010 (0.021)
Average main chain B values (Å^2)	36.2	40.9
Average side chain B (Å^2)	42.5	47.4
Average ligand B (Å^2)	48.6	51.2
Preferred regions	822	835
Allowed regions	24	24
Outliers	4	2

[a] values in parentheses correspond to the highest resolution shell

[b] R_{merge} is defined as $100\times\Sigma\left|I-<I>\right|/\Sigma I$, where I is the intensity of the reflection

[c] R.m.s. deviations from ideal geometry (target values are given in parentheses)

**Supplementary Table 2. Cell dimensions of apo-CeuE, [Fe^{III}(AZOTO)]$^{2-}$⊂CeuE and [Fe^{III}(11)Cp*Ir^{III}]⊂CeuE.**

	a / Å	b / Å	c / Å	α / °	β / °	γ / °
Apo CeuE	56.95	62.74	67.98	82.19	76.74	75.96
[Fe^{III}(AZOTO)]$^{2-}$	58.14	63.39	67.64	82.73	76.37	79.03
[Fe^{III}(**11**)Cp*Ir^{III}]	56.68	62.83	68.24	87.44	77.00	79.08

Supplementary Table 3. Crystallographic data for [Cp*Ir^{III}(6)Cl] (13).

CCDC deposition number	1551724
Empirical formula	$C_{23}H_{25}ClIrN_3O_2S$
Formula weight	635.17
Temperature/K	110.00(10)
Crystal system	monoclinic
Space group	P2$_1$/c
a/Å	13.9332(2)
b/Å	9.46210(10)
c/Å	17.7187(2)
α/°	90
β/°	100.3950(10)
γ/°	90
Volume/Å^3	2297.65(5)
Z	4
ρ$_{calc}$g/cm^3	1.836
μ/mm^{-1}	6.043
F(000)	1240.0

Crystal size/mm^3	0.502 × 0.238 × 0.062
Radiation	MoK$_\alpha$ (λ = 0.71073)
2Θ range for data collection/°	6.65 to 64.388
Index ranges	-20 ≤ h ≤ 20, -12 ≤ k ≤ 14, -26 ≤ l ≤ 26
Reflections collected	26287
Independent reflections	7388 [R_{int} = 0.0472, R_{sigma} = 0.0497]
Data/restraints/parameters	7388/48/305
Goodness-of-fit on F^2	1.071
Final R indexes [I>=2σ (I)]	R_1 = 0.0335, wR_2 = 0.0697
Final R indexes [all data]	R_1 = 0.0504, wR_2 = 0.0795
Largest diff. peak/hole / e Å^{-3}	2.33/-1.44

Supplementary Figures
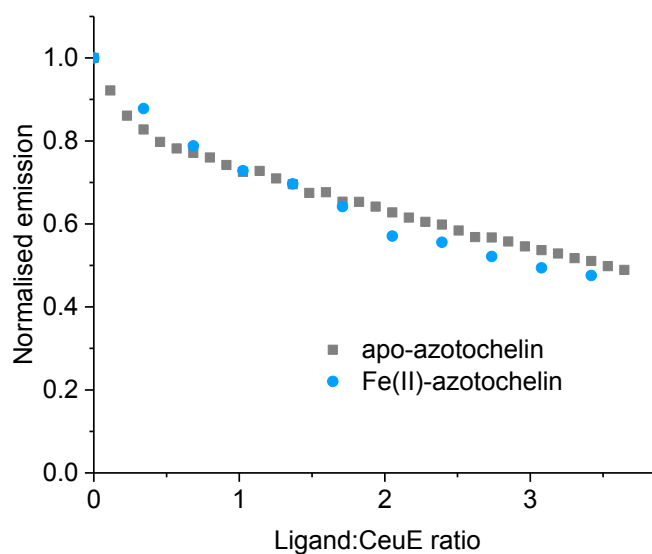
Supplementary Figure 1. Intrinsic fluorescent quenching observed upon addition of apo-azotochelin (grey squares) and Fe(II)-azotochelin (blue circles) to CeuE (40 mM Tris-Cl pH 7.5, 150 mM NaCl).
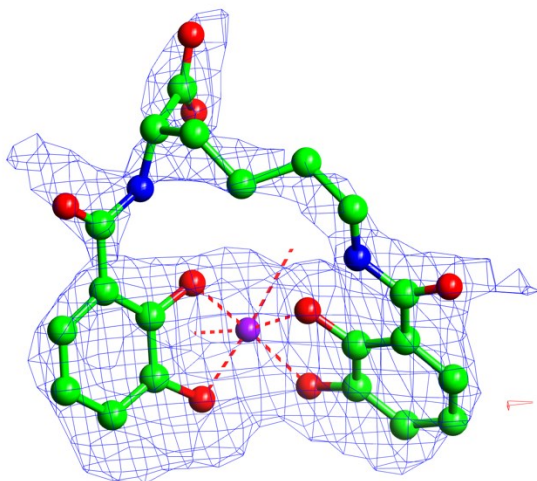
Supplementary Figure 2. The maximum likelihood difference map for azotochelin and Fe (purple) bound to Chain B. The phases were calculated from the protein model prior to introduction of the ligand, and the map is contoured at the 2σ level. The model is from the refined structure of the complex. For clarity, the H227 and Y288 residues completing the coordination of the iron are not shown.
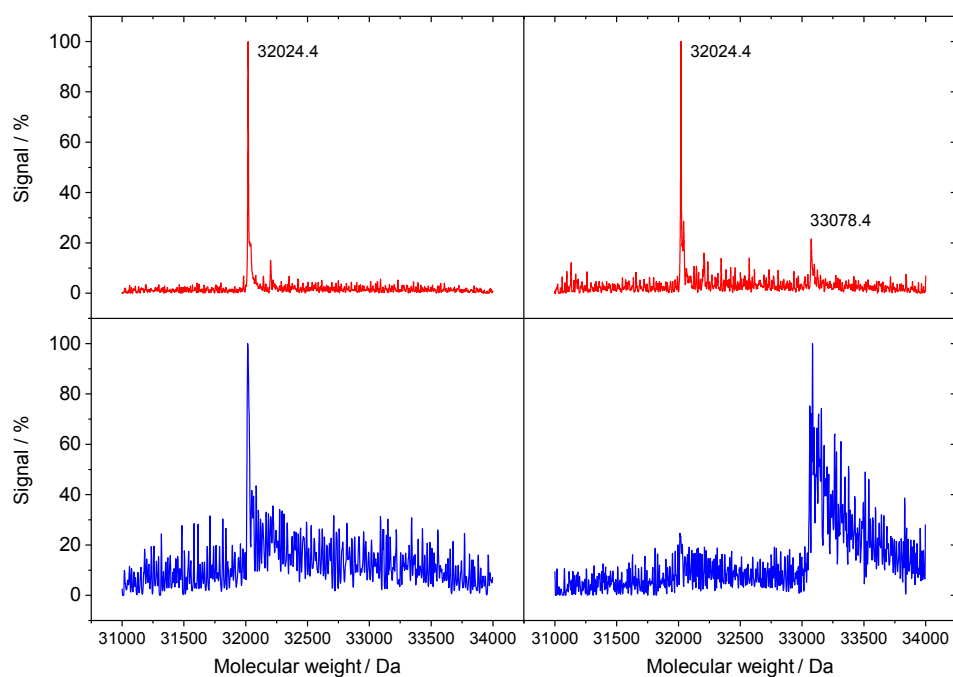

**Supplementary Figure 3.** ESI-MS of CeuE in the absence (left) or presence (right)

of $[Fe^{III}(\mathbf{11})Cp^*Ir^{III}Cl]^-$. Raw m/z data were processed to yield the spectra. The upper traces for each sample (red) were derived from the 810-2000 m/z range of the raw data (usually associated with unfolded protein). The lower traces for each sample (blue) were derived from the 2000-3400 m/z rage of the raw data.
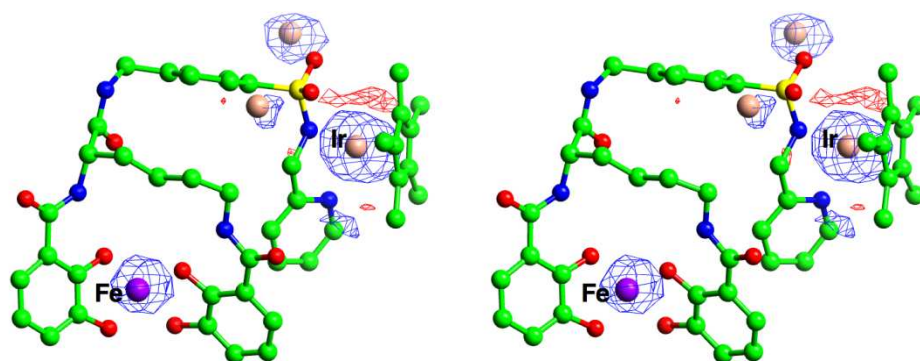
Supplementary Figure 4. Stereo view of the anomalous difference map around the bound [Fe(**11**)Cp*Ir] in Chain C. The phases were calculated from the protein model prior to introduction of the ligand, and the maximum likelihood anomalous map is contoured at the 4σ level. The model is from the refined structure of the complex. The iron atom is coloured purple, the iridium atoms salmon, with the major site labelled. The peak corresponding to the iron has a height of 12 σ, with a much bigger peak of 31 σ assigned to the major iridium site. There are two other peaks in the vicinity with heights about 5 and 8 σ, assigned as alternative iridium locations.
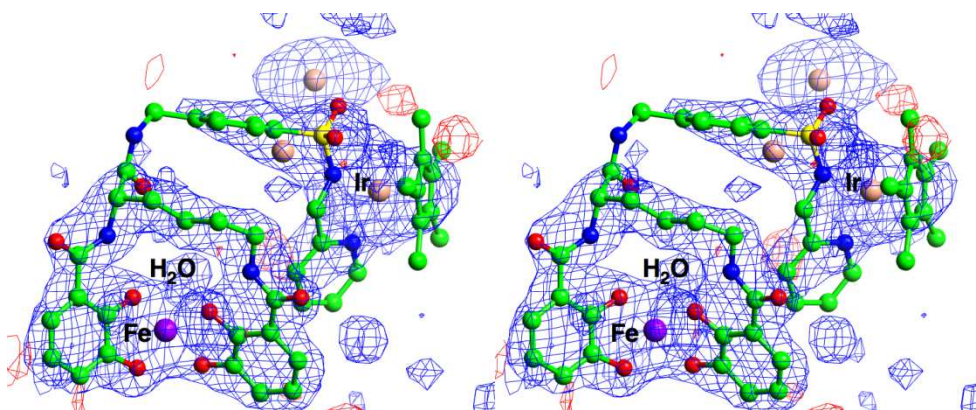
Supplementary Figure 5. Stereo view of the maximum likelihood difference map for the conjugate [Fe(**11**)Cp*Ir] with iron (purple) and iridium (salmon) bound to Chain C. The phases were calculated from the protein model prior to introduction of the ligand, and the map is contoured at the 2σ level. The model is from the refined structure of the complex. The water replacing His227 as the sixth iron ligand is shown. The major iridium site is labelled.
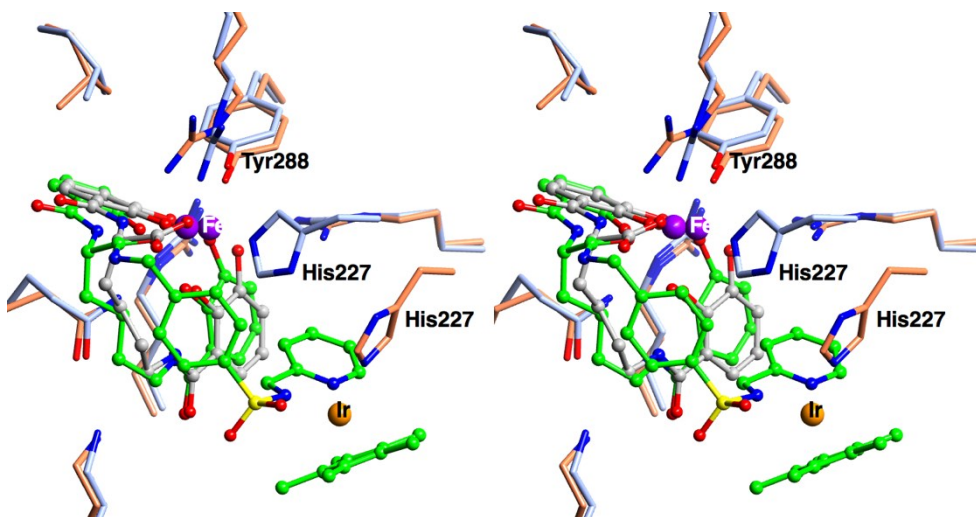

Supplementary Figure 6. Stereo view of the structural overlay of the binding sites in $[Fe^{III}(AZOTO)]^{2-} \subset CeuE$ (grey) and $[Fe^{III}(\mathbf{11})Cp*Ir^{III}] \subset CeuE$ (protein with atoms in coral, ligand with carbons in green and ball and stick). Only the major Ir site is shown, as a sphere. The movement of His227 from its position binding the Fe in the

azotochelin complex is clear. The positions of the other neighbouring residues are essentially unchanged.
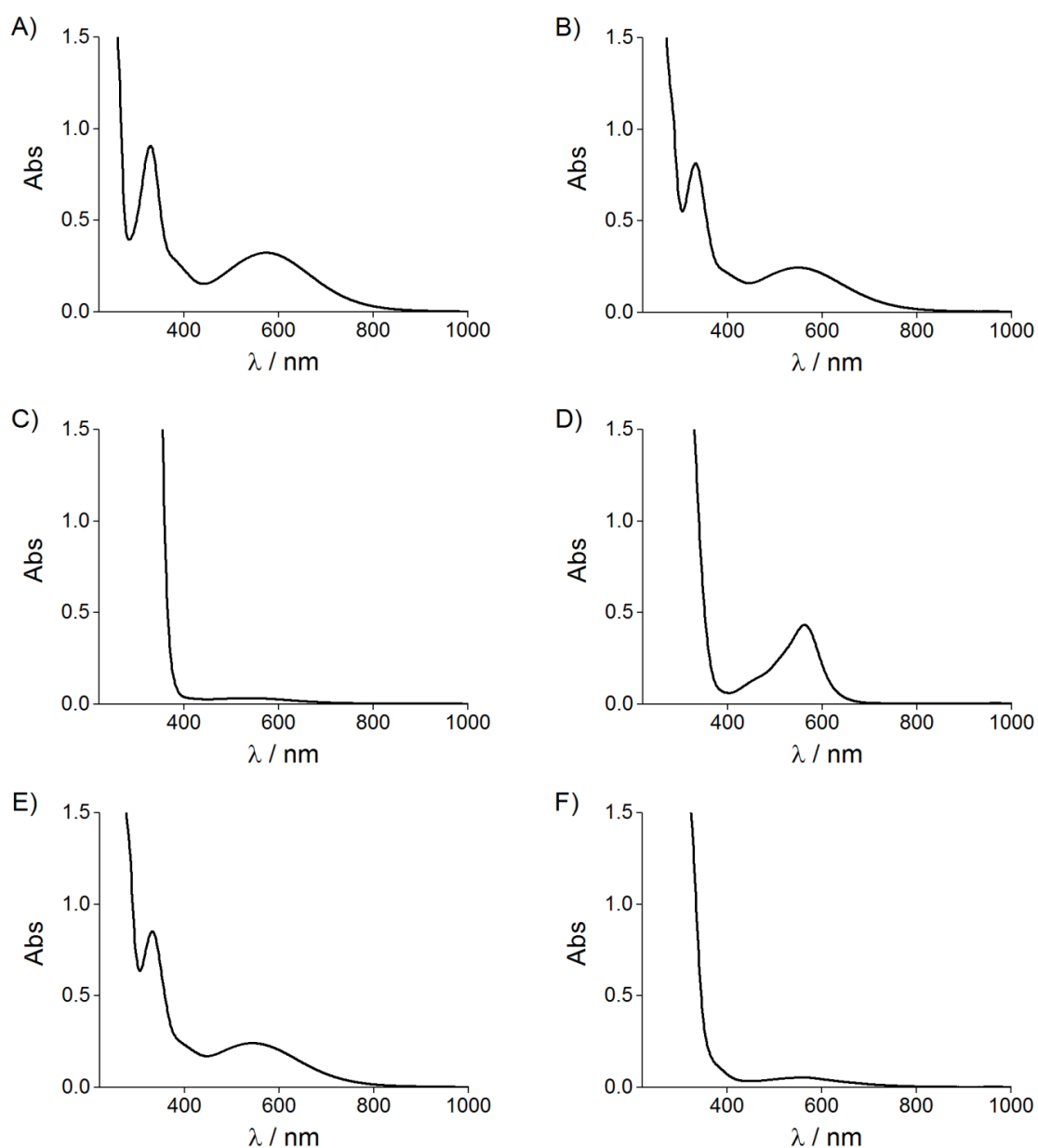
Supplementary Figure 7. UV-visible absorbance spectra recorded as part of the reversibility study of $[Fe^{III}(AZOTO)]^{2-} \subset CeuE$. A: $[Fe^{III}(AZOTO)]^{2-}$; B: $[Fe^{III}(AZOTO)]^{2-} \subset CeuE$; C: reduced sample, $[Fe^{II}(AZOTO)]^{2-} \subset CeuE$; D: aliquot of C with Fe(II)

indicator ferrozine – positive result for Fe(II); E: oxidation of C; F: aliquot of E with

Fe(II) indicator ferrozine – negative result for Fe(II).

A)

B)
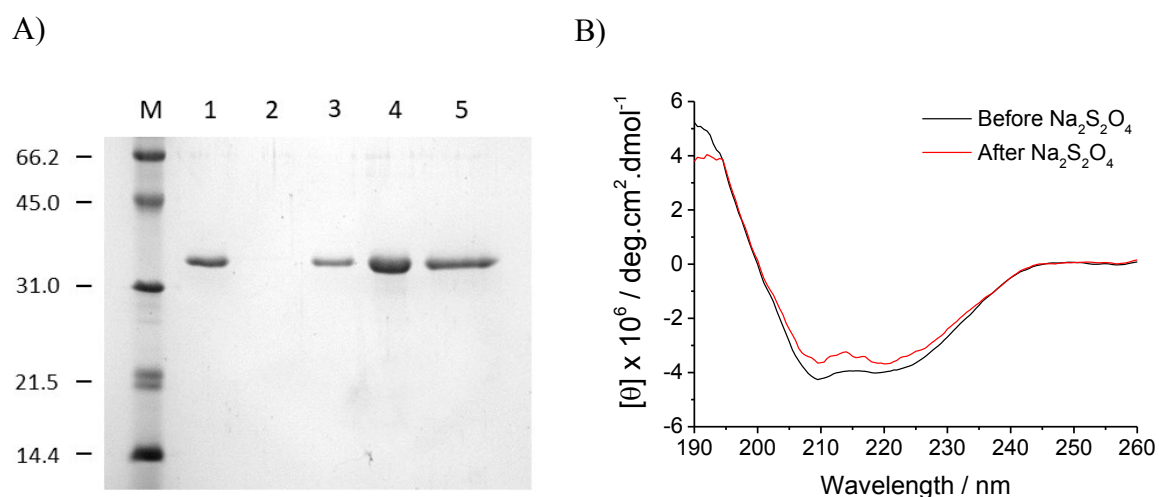
Supplementary Figure 8. A) SDS-PAGE of CeuE as part of the reversibility study.

Lane M: low molecular weight protein marker, Lane 1: [Fe^{III}(**11**)Cp*Ir^{III}]⊂CeuE before

reduction, Lane 2: Flow through of [Fe^{III}(**11**)Cp*Ir^{III}]⊂CeuE sample after addition of 10

mM Na$_2$S$_2$O$_4$ and centrifugation through centrifugal concentrator, Lane 3: Retained

fraction of the same sample as lane 2, Lane 4: Addition of fresh

[Fe^{III}(solv)$_2$(**11**)Cp*Ir^{III}Cl]$^-$ to the retained fraction to reassemble artificial metalloenzyme,

Lane 5: Sample of reassembled metalloenzyme after 72 h incubation in transfer

hydrogenation reaction. B) UV-CD spectrum of [Fe^{III}(**11**)Cp*Ir^{III}]⊂CeuE before and
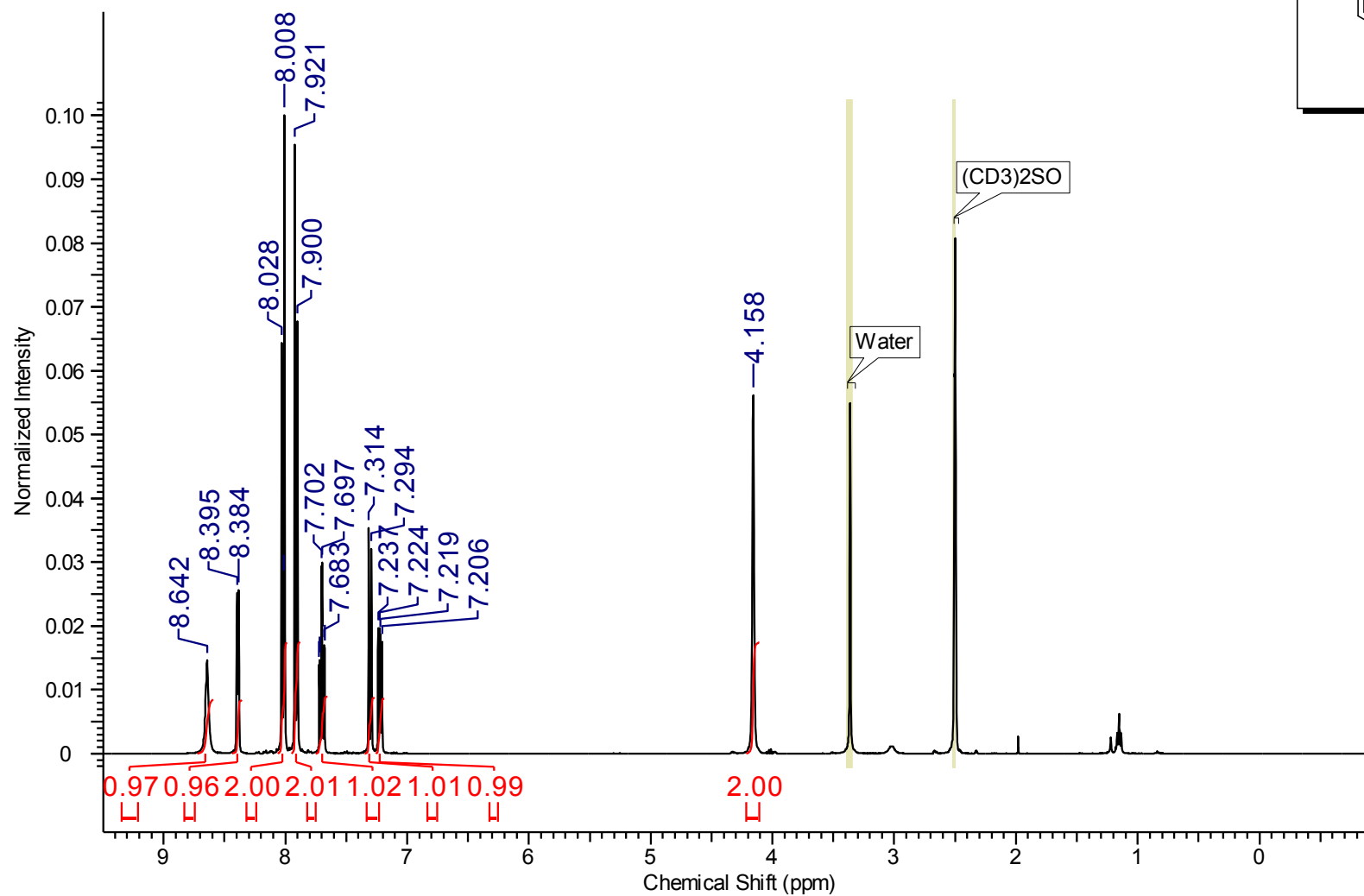
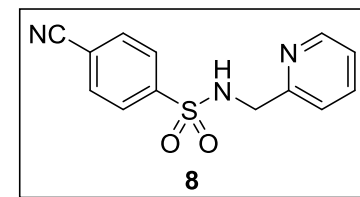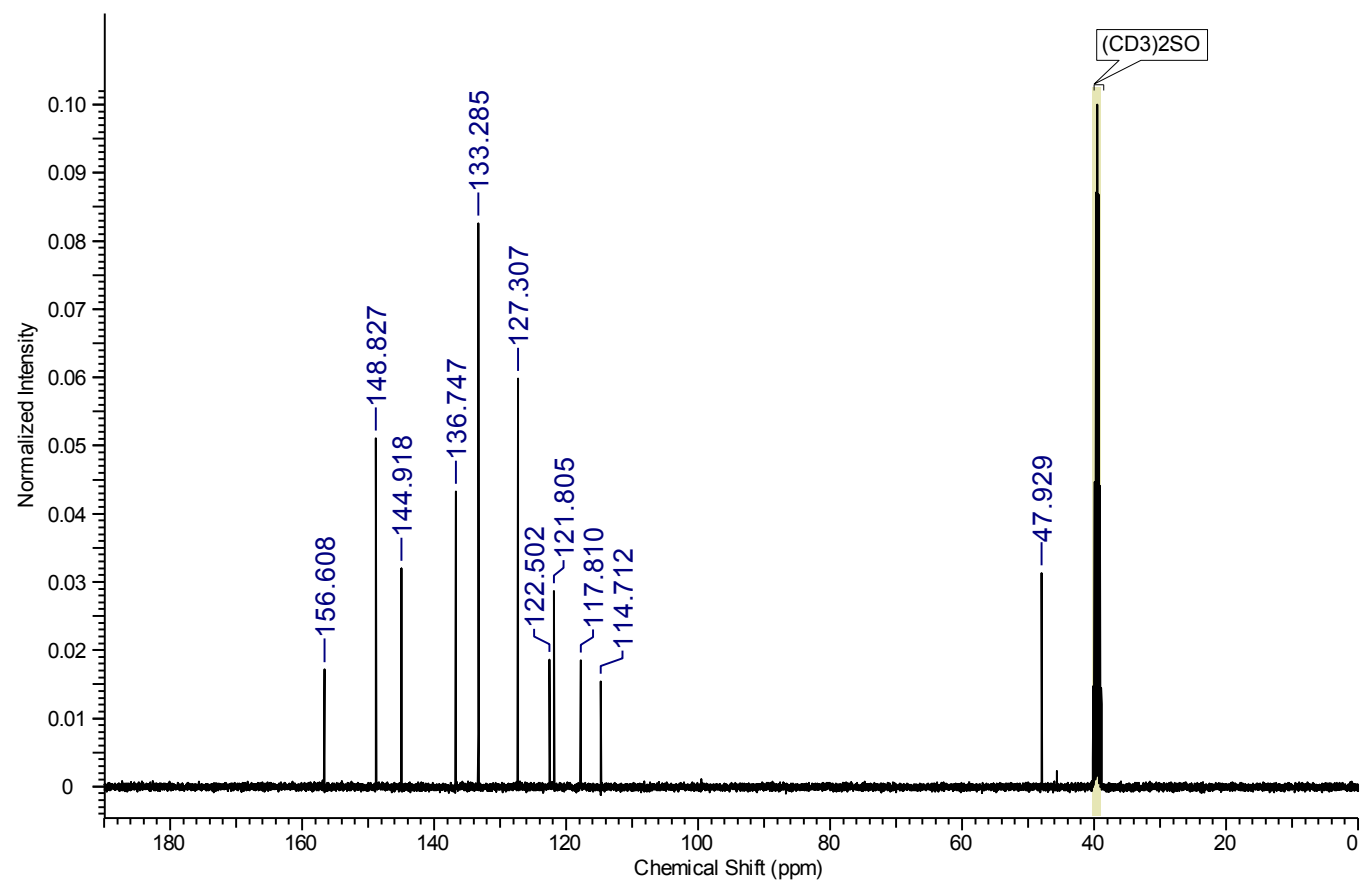after addition of 10 mM Na$_2$S$_2$O$_4$.

A)

B)
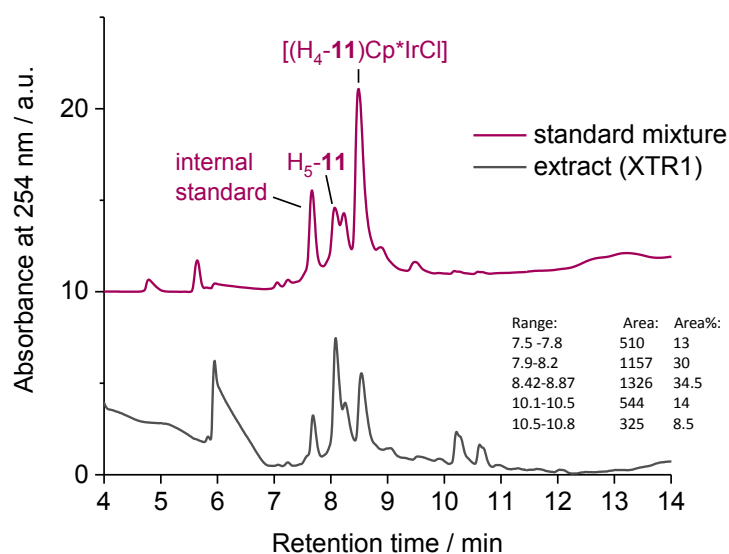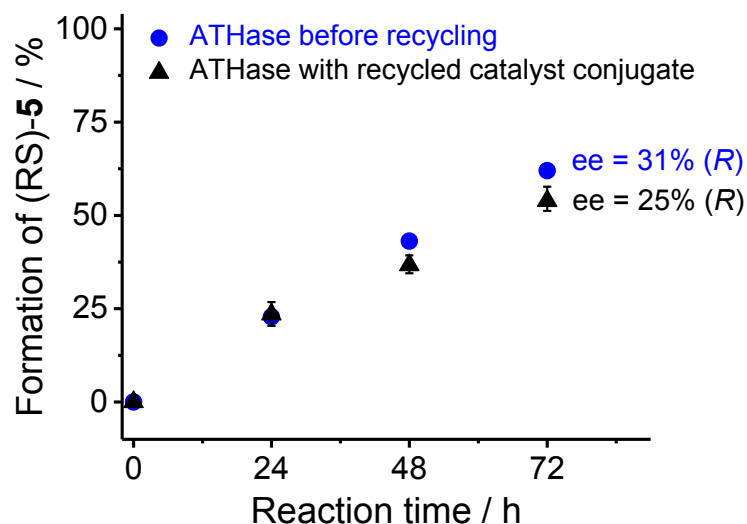
Supplementary Figure 9. A) HPLC trace of the organic extract (black) and relevant standards (red). B) Kinetic profile for the formation of (*RS*)-**5** catalysed by the recycled conjugate in comparison the kinetic profile obtained with the ATHase before recycling (as in Fig. 6). Catalytic assay conditions as in Figure 6 (triplicate experiments with the recycled conjugate were performed using one batch of ATHase extract, error bars show min. and max. values).

^{1}H NMR - (CD$_3$)$_2$SO

8.642
8.395
8.384
8.028
8.008
7.921
7.900
7.702
7.697
7.683
7.314
7.294
7.237
7.224
7.219
7.206
4.158

Water
(CD3)2SO

0.97 0.96 2.00 2.01 1.02 1.01 0.99
2.00

Normalized Intensity

Chemical Shift (ppm)

8

¹³C{¹H} NMR - (CD₃)₂SO

$^{13}C\{^1H\}$ NMR - $(CD_3)_2SO$

^{1}H NMR - (CD$_3$)$_2$SO

(CD3)2SO

Water

8.435
8.433
8.425
8.423
7.749
7.734
7.713
7.520
7.499
7.366
7.347
7.237
4.037
3.774

1.00 3.15 1.97 1.08 1.08   1.97 1.97

Normalized Intensity

Chemical Shift (ppm)

9

$^{13}C\{^1H\}$ NMR - $(CD_3)_2SO$

(CD3)2SO

157.237
149.209
148.751
138.225
136.747
127.545
126.430
122.406
121.605
47.958
45.193

Normalized Intensity

Chemical Shift (ppm)

^{1}H NMR - CDCl$_3$

Normalized Intensity

8.444
8.426
8.396
8.385
7.719
7.698
7.458
7.405
7.294
7.289
CDCl3
7.086
7.105
7.123
6.237
5.144
5.046
4.467
4.451
4.406
4.390
4.177
4.171
3.162
3.146
3.129
3.113
1.716
1.697
1.357
1.265
1.247
Water
1.228
1.211
1.178
1.161
1.141

Chemical Shift (ppm)

1.00 1.00 0.97 2.03 1.99 1.09 1.95 3.13 6.40 0.94 3.99 1.99 2.05 1.11 1.82 1.94 2.02 1.05 4.24

10

BnO
BnO
O
NH
O
OBn
OBn
H
N
O
O
S
O
H
N
N

$^{13}C\{^1H\}$ NMR - CDCl$_3$

Normalized Intensity

Chemical Shift (ppm)

171.738
165.703
165.045
154.871
148.826
143.534
136.259
136.145
136.011
128.851
128.698
128.631
128.584
127.640
127.096
127.316
121.852
117.323
116.808
76.304
76.085
71.250
71.155
CDCl3
53.620
47.366
42.579
39.023
30.641
28.763
23.061

BnO
BnO
OBn
OBn
NH
NH
O
O
H
N
O
10
S
O
O
N
H
N

^{1}H NMR - CD$_3$OD

Water

CD3OD

Chemical Shift (ppm)

8.345, 8.333, 7.754, 7.733, 7.679, 7.434, 7.413, 7.362, 6.924, 6.710, 6.688, 6.668, 4.606, 4.592, 4.586, 4.448, 4.395, 4.148, 3.633, 3.615, 3.598, 3.385, 3.367, 1.988, 1.698, 1.680, 1.662, 1.194, 1.177, 1.160

0.85 1.79 0.83 1.87 1.90 1.91 2.03 2.02 1.00 1.92 1.86 1.78 2.10 1.88 2.33 2.17 2.79

11

$^{13}C\{^1H\}$ NMR - CD$_3$OD

Normalized Intensity

Chemical Shift (ppm)

173.404
170.191
169.819
156.890
148.900
148.204
145.867
139.098
137.458
127.637
126.922
118.502
118.283
117.320
115.747
115.451
57.012
53.980
42.176
38.810
31.325
28.722
23.135
17.051

CD3OD

11

^{1}H NMR - CDCl$_3$

Peaks: 8.543, 8.529, 8.164, 8.143, 7.741, 7.721, 7.586, 7.566, 7.293, 7.277, 7.249, 7.230 (CDCl3), 5.304, 4.870, 4.827, 4.558, 4.515, 1.762, 1.727 (Water)

Integrations: 1.04, 2.08, 1.03, 2.16, 0.65, 1.32, 1.03, 1.15, 15.53

Compound **12**

Normalized Intensity vs Chemical Shift (ppm)

Supplementary Figure 10. ^{1}H and ^{13}C NMR spectra of compounds 8-12.

^{13}C{^{1}H} NMR - CDCl$_3$

Peaks: 163.929, 151.496, 147.997, 138.481, 132.369, 129.175, 125.199, 120.717, 118.715, 114.072, 87.069, CDCl3, 57.778, 9.779

Compound **12**

Supplementary References

1 Letondor, C. *et al.* Artificial transfer hydrogenases based on the biotin−(strept)avidin technology: fine tuning the selectivity by saturation mutagenesis of the host protein. *J. Am. Chem. Soc.* **128**, 8320-8328 (2006).

2 Shende, V.S. *et al.* Asymmetric transfer hydrogenation of imines in water/methanol co-solvent system and mechanistic investigation by DFT study. *RSC Advances* **4**, 46351-46356 (2014).

3 Grajewska, A. & Rozwadowska, M.D. Total synthesis of (R)-(+)-salsolidine by hydride addition to (R)-N-tert-butanesulfinyl ketimine. *Tetrahedron: Asymmetry* **18**, 557-561 (2007).

4 Kuzmič, P. Program DYNAFIT for the analysis of enzyme kinetic data: application to HIV proteinase. *Anal. Biochem.* **237**, 260-273 (1996).

5 Kabsch, W. XDS. *Acta Cryst. D.* **66**, 125-132 (2010).

6 Winter, G. xia2: an expert system for macromolecular crystallography data reduction. *J. Appl. Crystallogr.* **43**, 186-190 (2010).

7 Evans, P.R. & Murshudov, G.N. How good are my data and what is the resolution? *Acta Cryst. D.* **69**, 1204-1214 (2013).

8 Winn, M.D. *et al.* Overview of the CCP4 suite and current developments. *Acta Cryst. D.* **67**, 235-242 (2011).

9 Vagin, A. & Teplyakov, A. Molecular replacement with MOLREP. *Acta Cryst. D.* **66**, 22-25 (2010).

10   Murshudov, G.N. *et al.* REFMAC5 for the refinement of macromolecular crystal structures. *Acta Cryst. D.* **67**, 355-367 (2011).

11   Emsley, P., Lohkamp, B., Scott, W.G. & Cowtan, K. Features and development of Coot. *Acta Cryst. D.* **66**, 486-501 (2010).

12   Monnard, F.W. *et al.* Human carbonic anhydrase II as host protein for the creation of artificial metalloenzymes: the asymmetric transfer hydrogenation of imines. *Chem. Sci.* **4**, 3269-3274 (2013).

13   Dürrenberger, M. *et al.* Artificial transfer hydrogenases for the enantioselective reduction of cyclic imines. *Angew. Chem. Int. Ed.* **50**, 3026-3029 (2011).

14   Long, F. *et al.* AceDRG: a stereochemical description generator for ligands. *Acta Cryst. D.* **73**, 112-122 (2017).

15   Dolomanov, O. V., Bourhis, L. J., Gildea, R. J., Howared, J. A. K., Puschmann, H. OLEX2: a complete structure solution, refenement and analysis program. *J. Appl. Cryst.* **42**, 339-341 (2009).